Developing vanadium redox flow technology on a 9-kW 26-kWh industrial scale test facility: design review and early experiments

Massimo Guarnieri[a], Andrea Trovò[a], Angelo D'Anzi[b], Piergiorgio Alotto[a]

[a]Department of Industrial Engineering – University of Padua, Padua, Italy

[b]StorEn, Stony Brook, NY-USA

Abstract Redox Flow Batteries (RFBs) have a strong potential for future stationary storage, in view of the rapid expansion of renewable energy sources and smart grids. Their development and future success largely depend on the research on new materials, namely electrolytic solutions, membranes and electrodes, which is typically conduced on small single cells. A vast literature on these topics already exists. However, also the technological development plays a fundamental role in view of the successful application of RFBs in large plants. Despite that, very little research is reported in literature on the technology of large RFB systems. This paper reports on the design, construction and early operation of a vanadium redox flow battery test facility of industrial size, dubbed IS-VRFB, where such technologies are developed and tested. In early experiments a peak power of 8.9 kW has been achieved with a stack specific power of 77 W kg^{-1}. The maximum tested current density of 635 mA cm^{-2} has been reached with a cell voltage of 0.5 V, indicating that higher values can be obtained. The test facility is ready to be complemented with advanced diagnostic devices, including multichannel electrochemical impedance spectroscopy for studying aging and discrepancies in the cell behaviors.

Keywords: Redox Flow Battery, Vanadium, Experimental flow battery, Industrial size test facility

1. Introduction

Electrical grids are becoming smart systems provided with distributed generation from photovoltaic (PV) systems, wind turbines (WT), and other intermittent renewable sources [1] [2]

[3]. Both in distributed installations, in the case of large grids, or in local installations, in the case of microgrids and nanogrids, energy storage will play a major role in coping with balancing source-load mismatches to avoid instabilities which can disrupt grid operations. In addition, it can provide a number of different services to improve the grid's economical and technical performance at levels unparalleled by traditional grids [1] [2] [3] [4]. These services call for energy storage systems (ESSs) with different ranges of power, response time, discharge duration, and storage duration [5] [6] [7] [8] [9]. They are often classified as power quality, in the case of fast operation times, and energy management, in the case of long times. The number of these services is increasing consistently, since new types of operation are continuously proposed and implemented. Notably, some Transmission System Operators (TSOs) have started requiring ESSs to contribute to primary and secondary regulation, which stress the advantage of fast responses and long discharge times at the same time [10] [11] [12]. Seasonal storage is another emerging service that aims at storing energy produced in the high-generation months for later use it in other months of the year.

Different storage technologies can provide these services and among them ElectroChemical Energy Storage (ECES) systems [13] [14] appear as the most promising, because their modularity allows a wide power and energy scalability, resulting in power sizing of kilowatt-to-megawatt and discharge duration of minutes-to-hours [15] [16], covering ranges which are precluded to other commercial technologies [17] and making them particularly suitable for smart grids, minigrids and microgrids, not to mention electric mobility. ECESs are also convenient for their site versatility, near-zero environmental impact, static structure, silent and simple operation. Several ECESs, consist of "closed" or "solid-state" batteries in which the electrodes (based on lithium, sodium, nickel, lead, …) perform a double function: hosting the electrochemical conversion reactions and storing the converted energy. Power and energy are consequently reciprocally bonded, resulting in compact systems, but with short discharge times at maximum power. Another ECES family consists of "open" devices, in which fluid reagents are fed in/taken

from the electrodes, thus allowing to store the converted energy outside the cells. These devices are Redox Flow Batteries (RFBs) and hydrogen-based ESSs, consisting of an electrolyzer, a hydrogen reservoir and a fuel cell (ELHFC) [18] [19]. The open structure provides these ECESs with the tremendous advantage of decoupling power and energy, allowing for discharge duration sized at will. The stored energy can be increased at a limited cost, simply by adding more reacting fluid, in larger tanks. RFBs and ELHFCs also exhibit a very wide scalability, more than Li-ion, which, due to the limited size of the single cells, pose safety issues when assembled in very large number to build large plants. Nevertheless, many comparative studies on ECES published to date fail to provide complete assessments and often disregard RFBs, or pay a very limited attention to their advantages [20], despite several large all Vanadium RFB (VRFB) systems in the megawatt-megawatthour size have been put into service in some countries and China is installing a 200-MW 800-MWh VRFB station [21] that is by far the largest ECES ever built with a size comparable to several pumped-hydro or compressed-air energy storage systems.

VRFBs exhibit a notable combination of advantages. When in standby they are able of fast responses, in the order of a few milliseconds. They can be overloaded (in the order of 50%) for a few seconds which allow to face several power quality grid services. They can provide long discharges by properly sizing the solution volumes which is convenient for energy management grid services. Moreover they can store energy in their tanks for very long times when in off mode which allows for services like seasonal storage. This combination of features poses them in a very competitive position in view of future stationary storage demand. Since VRFBs use vanadium ions on both electrodes, they do not undergo cross-contamination, which allows extremely long calendar life (>20 years) and cycle life (>20,000 cycles). Their levelized cost is thus very low, also below 5 c€ kWh^{-1} $cycle^{-1}$, that is the present EU target for ECEDs. Working between 10°C and 50°C, they do not present major thermal conditioning requirements. Neither do they suffer from severe safety issues, because they use liquid solutions at atmospheric pressure.

On the other hand, VRFBs have some weaknesses with respect to other ECES, which call for research and development. The major challenges regard increasing energy and power densities and widening temperature stability. Some loss effects must also be addressed in order to increase the round-trip efficiency, including species crossover, solution pressure drops and shunt currents management [22].

2. Status of VRFB research

RFB is not a new concept. After pioneering work by a NASA research group in the 1970s [23] and independently and simultaneously by Pelligri and Spaziante in 1978 [24] the Vanadium Redox Flow Battery was first successfully demonstrated by Maria Skyllas Kazacos in the 1980s, with a design patented in 1986 [25] [26]. The following technology developments in Australia, Japan and US led to a first generation of commercial plants in the class of hundred kilowatts to a few megawatthours [16], peaking with the 4-MW/6-MWh station installed by Sumitomo Electric Industries (SEI) for Electric Power Development Co in Tomamae, Hokkaido, Japan, in 2005. Even though not completely competitive, those ESSs triggered an increasing interest toward the technology and more research groups started working on the VRFB concept, in order to improve its performance. RFBs based on other chemistries were also increasingly studied in several laboratories. Their pivotal targets are the developments of new materials, capable of overcoming RFB's weaknesses. New electrolytic solutions are being developed to store higher energy densities [27] [28] [29] [30] [31] and exhibit longer cycle lives (except VRFB, whose life in excess of 20.000 cycles in unparalleled among other ECESs); new and cheaper membrane are needed to reduce species crossover while presenting lower ohmic resistance [32] [33] [34] [35]; advanced porous electrodes, possibly enriched with inexpensive electrocatalysts, are being conceived with the aim of increasing electrochemical activity and reduce fluid-dynamic drag [36] [37] [38] [39] [40]; advanced fluid distribution design in the cell electrodes and current collector aims at achieving lower concentration losses [41] [42] [43]. These researches are typically developed on

small-size cells with active areas of 5–10 cm^2 and short stacks made of few small cells, which allow to experiment at relatively small expenses. Excellent results have already been achieved [44], but concerns remain on their transferability to commercial-size stacks, formed by several tens of cells with large active areas, in the order of some hundred square centimeters. From this point of view, testing new materials and architectures in a commercial-scale test facility operated in laboratory-controlled conditions has a strategic value. Nevertheless, due to the costs of such large experimental facilities, very few are operated worldwide and even less are reported in the scientific literature [45] [46] [47]. Indeed according to the recent authoritative review [48] "… the majority of publications have been restricted to short term studies of small electrodes in the laboratory; very few contributions have considered pilot-scale devices and the effect of cell design, electrode structure, reaction environment and operational conditions on performance. …"

For the sake of example, Fraunhofer ICT, Pfinztal, Germany, is experimenting on a system with a 4-kW stack [49] [50] and Hoseo University, Asan, South Korea, has developed a 10-kW 31-cell 2714-cm^2 experimental stack, recently reporting a top current density of 90 mA cm^{-2} [51], whereas 160 mA cm^{-2} for a 15-cell 780-cm^2 stack are presented in [52]. Dalian Institute of Chemical Physics, China, has developed a facility for testing several kW-scale stacks at a time, but it has not been reported in the literature, to our knowledge.

3. The IS-VRFB experiment at UNIPD - general description

The aim of this work is to present the design, construction and testing of a 9-kW/26-kWh Vanadium Redox Flow Battery provided with a stack architecture directly transferable to industrial production and that is fully instrumented for measurement campaigns in laboratory controlled conditions. This Industrial-Scale VRFB (IS-VRFB) test facility has been recently put into operation at the Electrochemical Energy Storage and Conversion Laboratory of the University of Padua (UNIPD). It consists of a 40-cell stack with a 600-cm^2 active area, conceived to deliver a power of 4 kW, and two 550-L 26-kWh vanadium solution tanks (Figure 1).

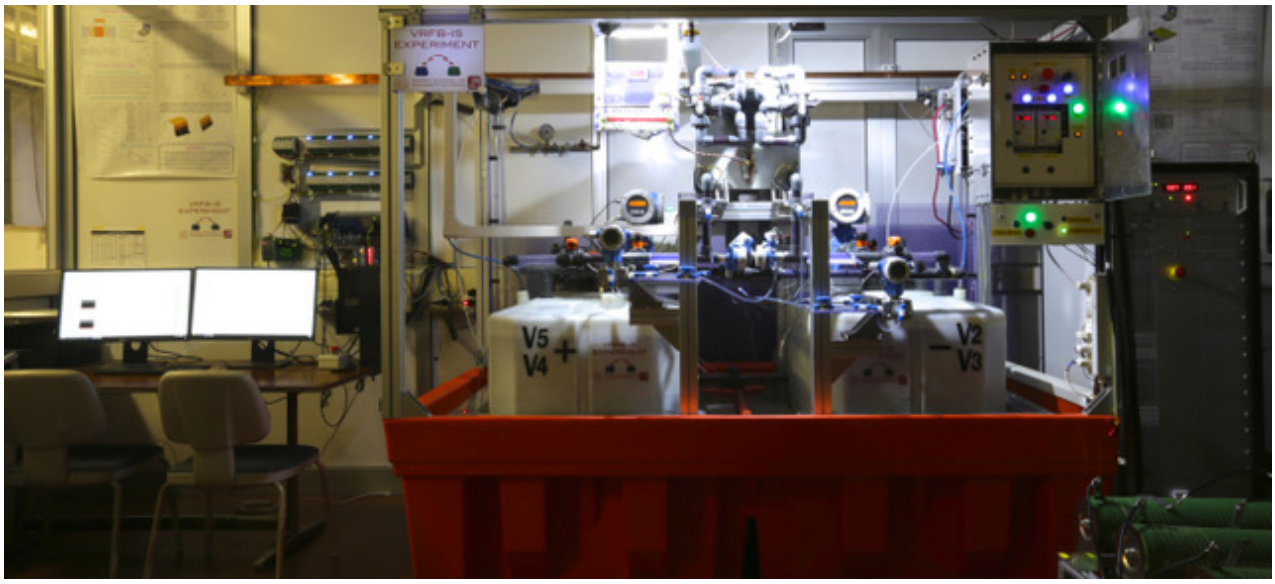

Figure 1. The IS-VRFB test facility

Table 1: IS-VRFB test facility features

Design parameter		
Number of cells	40	
Cell active area	30 × 20 cm^2	
Tank volume	2 × 550 L	
Sulfuric acid concentration	4.5 M	
Vanadium concentration	1.6 M	
Performance	**Design rating**	**Present top performance**
Stored energy	26 kWh	26 kWh
Stack OCV at SOC=10%,50%,90%	50.3 V, 54.8 V, 59.3 V	50.3 V, 54.8 V, 59.3 V
Top current	72 A	400 A
Residual voltage at top current		18.5 V
Peak power at SOC=90%	4000 W	8900 W
Top current density	120 mA cm^{-2}	665 mA cm^{-2}
Peak cell power density at SOC=90%	166 mW cm^{-2}	370 mW cm^{-2}

The main parameters are reported in Table 1. The design ratings were defined as expected performance based on recent scientific literature. A current density of 120 mA cm^{-2} was considered a reasonable figure in this phase, in view of the fact that the original treatment of the porous electrodes had not yet been checked on the large scale. The "present top performance" reported in the table are the values actually achieved in the early experimental campaign, and do not represent the effective stack limits which have yet to be explored.

The layout has been conceived for high accessibility, with the stack placed in an open space over the two tanks, which are set side by side (Figure 2). The pumps for circulating the solutions are located in the back, at a level that ensures easy triggering, while the inverters driving the pump motors are placed in the front electric panel, for easy access to the local controls. Each hydraulic circuit is equipped with valves for fast maintenance operation. The tanks are hermetically sealed and their residual volumes are filled with inert gas to prevent vanadium species from atmospheric oxygen contamination. Charge and discharge power control is provided by the Power Management System (PMS), which consists of a two-quadrant static converter that can be controlled both locally and remotely by the system supervisor. The plant is fully instrumented with electrical, thermal and fluid-dynamic probes. A flexible Battery Management System (BMS), namely the System Supervisor, has been built around a desktop computer with a Labview environment and a National Instruments (NI) compact data acquisition (Compact DAQ) interface that allows fully customizable high-level SCADA-like (Supervisory Control And Data Acquisition) data management and experiment control. Instrumentation includes multichannel electrochemical impedance spectroscopy (EIS) of the cells. High operation safety is ensured by the BMS in combination with a Surveillance System (SS) built around a Programmable Logic Controller (PLC) and provided with valve-status and flow-rate sensors. The system is designed for future expansions and upgrades. In particular, the hydraulic circuits are provided with ports for installing small stacks in which new materials and cell architectures can be tested before being used in a future upgraded larger stack.

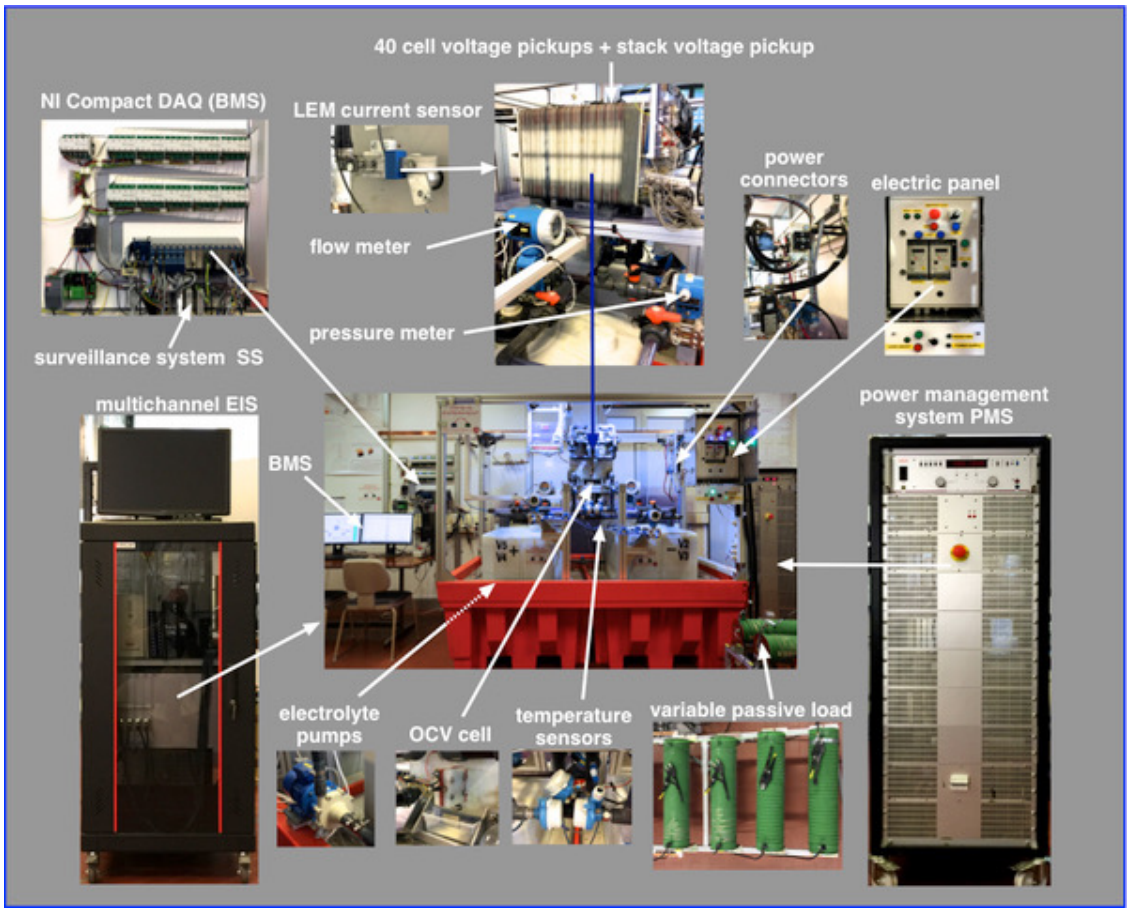

Figure 2. The IS-VRFB test facility and its main components

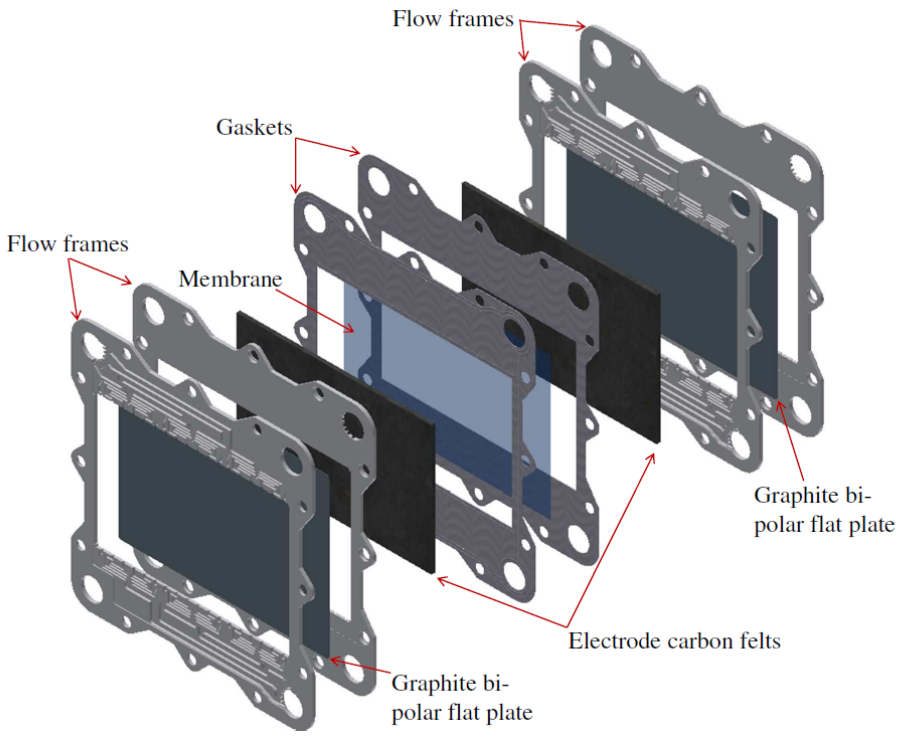

Figure 3. Cell configuration

4. Stack

The stack is the energy conversion device. It is the most important and complex part of a VRFB system and its design requires skills in electrochemistry, mechanical engineering, material science, chemistry, and computational modeling and simulation. Each electrochemical cell forming the stack is made of two porous electrodes separated by a polymeric membrane and fed with the electrolytic solutions (Figure 3). The IS-VRFB stack follows a conventional design with the cells fed hydraulically in parallel and connected electrically in series. At this aim, the cells are interleaved with frames encasing conducting plates (bipolar plates), which work as current collectors interconnecting electrically the cells while separating the solutions of different polarity [53], which is often reported as the most advantageous configuration.

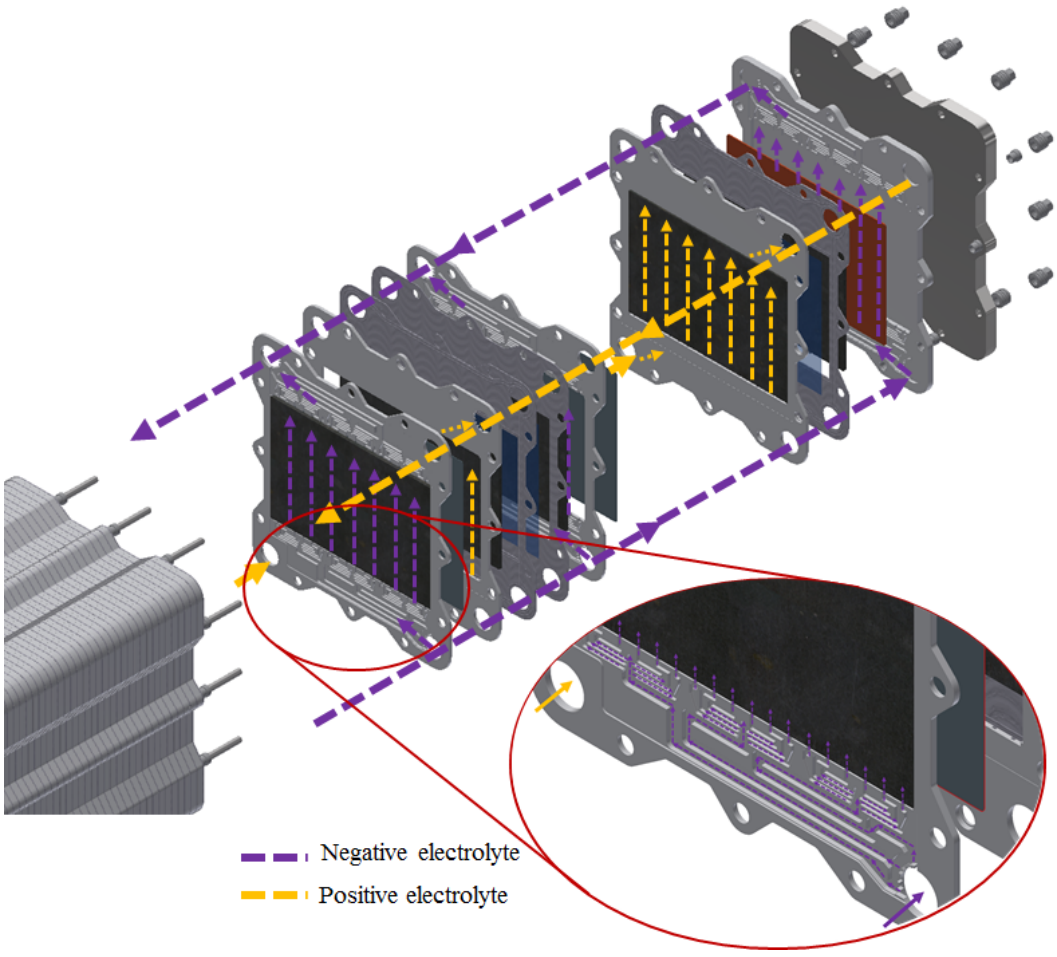

Figure 4. Internal stack hydraulic configuration

The IS-VRFB cells follow a conventional flow-through architecture, with flat current collectors and the electrolytic solutions permeating into the porous electrodes from one side to the opposite one (Figure 4). This design requires thicker electrodes in order to limit their pressure drop and results in relatively large ohmic losses [54]. 5.7-mm thick (after compression) graphite felt electrodes (Beijing Great Wall, China) and a Nafion® 212 membrane have been chosen for IS-VRFB. Before assembly the felts have undergone a series of thermochemical treatments for enhancing their electrochemical performance. At each electrode side the solutions are distributed through ramified channels grooved in the frames (hence flow frames) which follow an equal path length (EPL) design. This flow frame pattern was designed after hydrodynamics simulations performed with Fluent CFD and in-house computational tools [53] [55]. Results showed that the flow frame design ensures a uniform reactant flow throughout the electrodes, without stagnation zones. In both electrodes, the solutions flow from the lower manifold to upper one, to facilitate the removal of bubbles which could develop [48].

The cell and frame design, that was developed in view of potential series production, follows a modular concept that resorts to different materials and aims at easy manufacturing and reliable assembly. From the mechanical point of view the most critical component is the flow frame which can potentially cause solution leakages, both internal and between frames. This is a known issue of VRFBs that has not been definitely addressed despite the research carried out [56] [57] [58] [59]. The IS-VRFB frame consists of two identical half-frames cut from a 5-mm polypropylene (PP) plate and engraved with flow channels at a CNC machine, thus preventing shrinking problems of a cheaper hot molding process. Two half-frames have been assembled face to face with the flat graphite plate forming the bipolar plate in between. Frame sealing has been provided by acetic silicon. Each cell consisting of the two electrodes with the interleaved membrane has been assembled between two frames. Ethylene propylene diene monomer (EPDM) gaskets have been interposed between frames. Hydraulic sealing has been ensured by the gasket

compression provided by twelve threaded rods with nuts and cup springs which compress the two thick steel endplates.

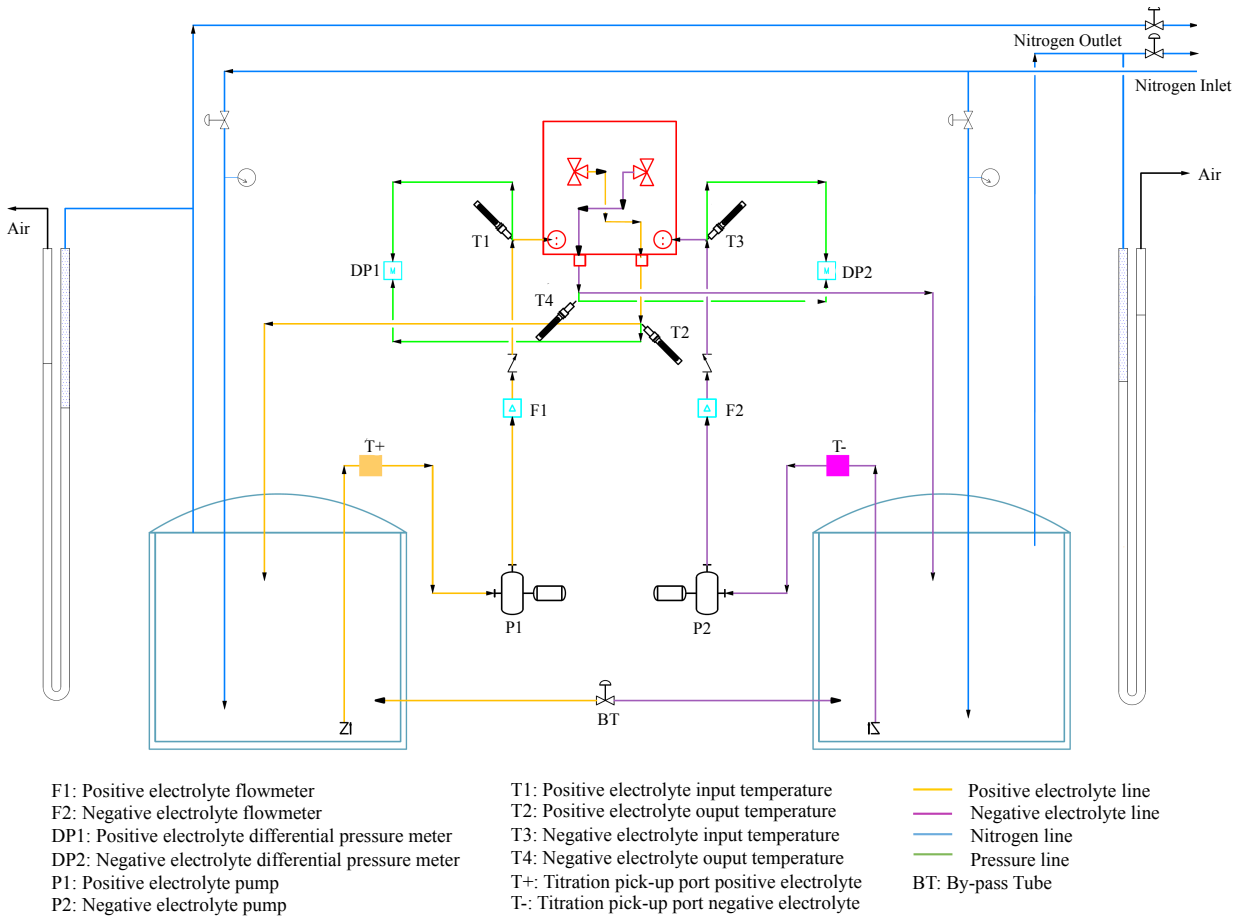

Figure 5. IS-VRFB P&ID (piping and instrumentation diagram)

5. Hydraulic circuits

Figure 5 shows the P&ID (piping and instrumentation diagram) of the two hydraulic circuits, each including tank, pump, piping and valves for fast maintenance. All components that have the parts exposed to the electrolytes are made of acid tolerant materials, in particular polyethylene (PE) and polyvinylchloride (PVC), to exclude corrosion issues. The two PE tanks storing the solutions are provided with reinforcement steel belts to prevent bulging and are placed inside a containment basin, to avoid any dispersion in the unlikely event of a leak. The PVC pipes include some transparent segments to allow a direct visual inspection of the solution flow and color, which provides an immediate indication of the solution state of charge (SOC). A by-pass

pipeline provided with a manual valve allows balancing the level in the two tanks and eliminating any pressure difference that can arise from variations in the electrolyte volumes because of ion and water crossover through the cell membranes [52]. The two circuits have been equipped with pick-up ports for collecting solution samples without opening the piping, in order to perform physical-chemical tests such as potentiometric titration.

5.1. Feedback controlled pumps

The two centrifugal pumps for circulating the solutions (PMD-641 by Sanso) have PVC stator and rotor, the latter being magnetically driven by a three-phase squirrel-cage induction motor. Two solid-state inverters (DC1 by Eaton) power the motors at variable-frequencies under a feedback control, in order to operate the pumps at controlled flow rates. The pumps have been sized to provide solution flow rates Q_p = 29.5 L min^{-1} in excess of the minimum flow rates Q_r needed for the reaction stoichiometry ensuring a flow factor $\alpha = (Q_p/Q_r) > 10$ at maximum PMS current of 75 A and SOC value s = 50%.

5.2. Inert atmosphere and differential pressure gauge

A nitrogen feeding circuit excludes the presence of atmospheric oxygen in the tanks' residual volumes. A specially developed pressure gauge has been installed in each tank to generate and control a light nitrogen overpressure. It uses U-shaped transparent pipes filled with water which ensure accurate control of the overpressure, since a water level differences of 1 cm reveals an overpressure 1 mbar. The gauge also allows collecting and blowing out any secondary gas potentially evolved inside the tank, notably hydrogen.

6. Instrumentation

A number of physical measurements are picked up to be processed by the BMS. Two customized electromagnetic flowmeters (Proline Promag by Endress+Hauser) have been chosen to

perform accurate volumetric flow-rate measurements. Each flowmeter is provided with a couple of tantalum grounding disks for eliminating measurement disturbance from shunt currents in the conductive solutions, while resisting chemical aggression. Two customized differential pressure gauges (Deltabar PMD by Endress+Hauser) measure the solution pressure drops between the stack inlets and outlets. They have been assembled in an ad-hoc design with Galden®-filled piping for preventing any contact between gauge septa and electrolytic solutions. Four Resistance Temperature Detectors (RTDs) Pt-100 (TR11 by Endress+Hauser) measure the solution temperatures at the stack inlets and outlets. Their inspection wells have been designed for the accurate measurement of the temperatures in the solution mean flows. Forty-one pickups provide the individual cells and stack electric voltages in load conditions. An unloaded small cell has been installed and fed with the same solution flowing in the stack to provide the real-time open circuit voltage (OCV) measurement in any operating condition. Two current sensors (HAS 50-S and HAS 200-S by LEM) are used to measure the stack current with high accuracy at low and high load. An independent display visualizes the stack and cell voltages. Multichannel electrochemical impedance spectroscopy (EIS) is provided by an ad-hoc developed analyzer (Material Mates, Italy) for characterizing cell impedances in the frequency range 0–500 kHz aimed at studying discrepancies and ageing effects. All detected signals are conditioned, logged, and processed in the BMS as described in section 8. Table 2 provides the measurement ranges and accuracies.

Table 2: Measurement ranges and uncertainty of the IS-VRFB sensors

Measurement	**Sensor**	**Range**	**Total uncertainty (95% confidence level)**
Stack pressure drop	Differential pressure transducer (Endress Hauser Deltabar PMD 75)	0 ÷ 300 KPa	± 450 Pa
Electrolyte flow rate	Volumetric flow meter	0 ÷ 60 L min^{-1}	± 0.5 %

	(Endress Hauser Promag 50 P)		
Electrolyte temperature	RTD temperature sensor (Omnigrad M TR11)	$-50 \div 250$ °C	$\pm 0.15 + 0.002 \lvert T \rvert$ K
Stack current	Current transducer (LEM HASS 200-S)	$-600 \div 600$ A	± 1 %
Cell voltage	Analog to digital converter (National Instruments NI 9209)	$-10 \div 10$ V	± 0.097 %
Stack voltage	Stack voltage sensor (LEM CV 3-100/SP3)	$-130 \div 130$ V	± 0.2 %
Inverter and pump power	Power analyzer (Seneca Z203-1)	$0 \div 2500$ W	± 0.5 %

7. Power Management System (PMS)

The Power Management System (PMS) provides the electric power conditioning during charge and discharge. It consists of an AC/DC bidirectional static converter (Dana, Italy), that can be fully controlled both locally and remotely by the system supervisor. The PMS is provided with a protection circuit breaker and a step-down transformer that ensures galvanic insulation from the grid. The rated PMS voltage is 0–85 V DC, while the rated current is ±75A DC current/voltage profiles of the static converter are controlled by means of in-house algorithms implemented in the system supervisor, and updatable according to the experimental needs. A passive load consisting of four adjustable high-current resistors has been added to allow discharge currents up to 400 A. The PMS is connected to the stack through a remote-control switching system that allows commutating from the PMS to the passive load and fast disconnection in the case of a faulty condition.

8. Battery Management System (BMS)

VRFBs must be designed for automatic unmanned operation, especially if they have to be installed in remote sites involving little or no human intervention. The development of an efficient BMS that provides such features is a critical issue to guarantee successful operation [60]. In industrial VRFBs these functions should be provided by a low-cost PLC with well-tested software. In an experimental system, supervision functions can be more conveniently implemented in a flexible and expandable system, with advanced programming features and human-machine interface (HMI). The IS-VRFB BMS is built around a desktop computer equipped with a Labview environment and a National Instruments (NI) compact data acquisition (Compact DAQ) interface (Figure 6). Signal conditioning between stack and Compact DAQ includes cell voltage galvanic insulation based on optoisolators (Isoblock by Verivolt) and stack voltage galvanic insulation provided by a DC/DC transformer. Noise suppression is provided by a grounding system based on a thick copper equipotential bar providing common reference to all signals. The BMS in-house software manages all data acquisition, processing and logging, and performs the subsequent analyses. It also provides experiment control, i.e. the electrical, fluid-dynamic and thermal management by means of real-time procedures which use the real-time measurements for feedback control.

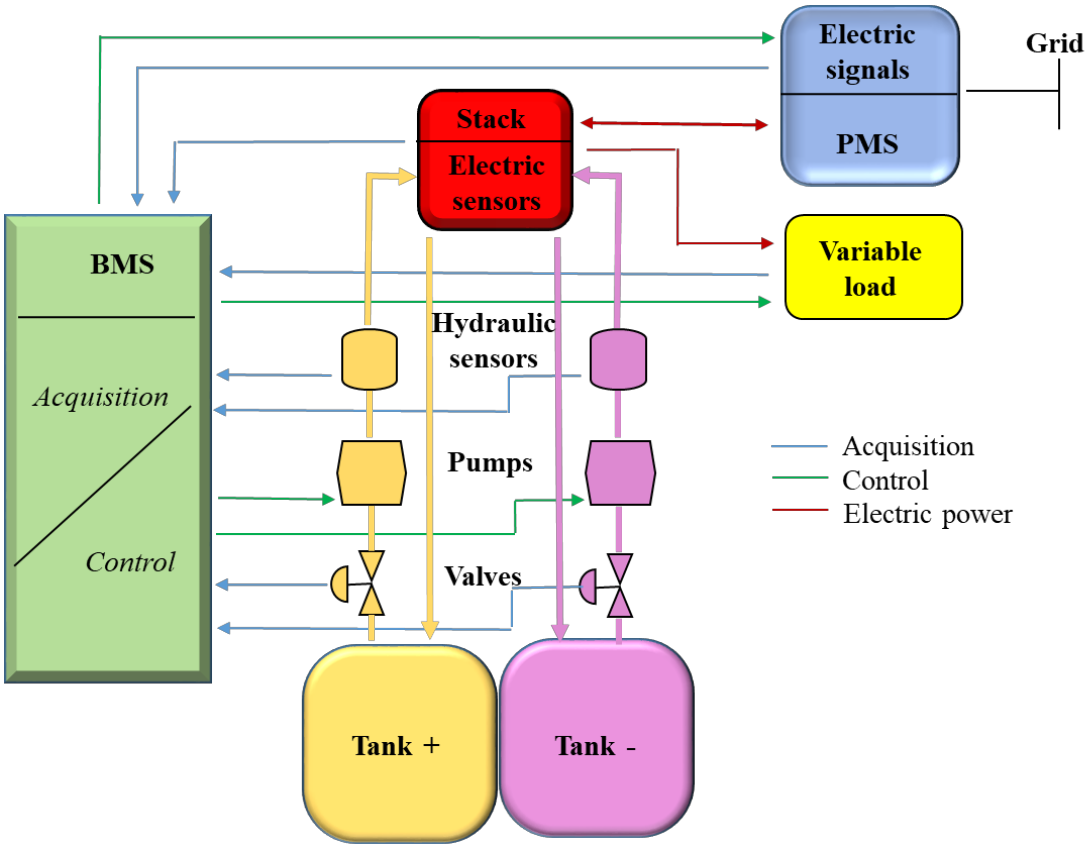

Figure 6. Interaction scheme between BMS and other IS-VRFB components

The system has been conceived and developed to guarantee high flexibility and wide capability of stack characterization, and its software allows designing the experimental sessions according to the evolution of the research program. In fact, LabView algorithms are continuously improved and developed to achieve the experimental goals.

For the sake of example, one LabView procedure of the BMS consists in managing inverters, pumps, and flowmeter signals so as the obtain the needed solution flow rates, according to the batteries electric performance and SOC. The BMS systematically computes the electric power $p(t)$ and the time evolutions of electric charge $\theta(t)$ [Ah] and energy $w(t)$ [Wh] flows by numerical integration of the stack current and voltage measurements. These figures allow further processing and analyses, notably, the computation of the stack coulombic η_Q, voltage η_V and energy η_W efficiencies [61].

$$\eta_\Theta = \frac{\Theta_d}{\Theta_c} \tag{1}$$

$$\eta_V = \frac{\overline{V_d}}{\overline{V_c}} \quad (2)$$

$$\eta_W = \frac{W_d}{W_c} \quad (3)$$

where Θ_c and Θ_d are the exchanged electrical charges during the whole charging T_c and discharging T_d times respectively, $\overline{V_c}$ and $\overline{V_d}$ are the corresponding average stack voltages, and W_c and W_d are the corresponding exchanged energies. Since the pump-driving inverters are fed from the grid, their energy consumptions in charge W_{pc} and discharge W_{pd} are measured by a specific power analyzer. The round trip efficiency (RTE) of the whole system is then computed as:

$$RTE = \frac{W_d - W_{pd}}{W_c + W_{pc}} \quad (4)$$

9. Surveillance System (SS)

The Surveillance System is responsible for protecting the system against the risks of improper operation. To this aim, it allows switching on the power only if the whole plant is in a standby condition with a number of checks in GO status. It also switches off the power if any check toggles to STOP, namely if any dangerous or faulty condition arises during operation. In order to ensure a high degree of reliability independently of BMS PC faults, it has been implemented with a separate PLC receiving signals from the valves which have been equipped with magnetic sensors for detecting any improper position. Safe operation in any condition is ensured by the combined actions of the SS and the BMS, which provide protection functions at different hierarchical levels. Some of these functions are described hereafter.

a. The PMS can be activated only if the two solution flows in the stack exceed the minimum values needed to sustain electrochemical reactions, avoiding the occurrence of improper reaction inside the cells, which can damage its components. These minimal flows depend on the electric current *i*, the SOC *s* and a minimal safe flow factor set at α_s = 3.5 [62]:

$$Q_{\min} = \begin{cases} \alpha_s \dfrac{N_{cell}}{c_v F} \dfrac{i}{(1-s)} & \text{in charge} \\ \alpha_s \dfrac{N_{cell}}{c_v F} \dfrac{i}{s} & \text{in discharge} \end{cases} \quad (5)$$

b. To avoid V_V precipitation at high SOC, a Labview algorithm that is active also in standby condition continuously monitors the stack temperatures provided by the RTD sensors and starts a stack washing cycle if temperatures exceed safe limits.
c. To avoid any mechanical issue in the hydraulic circuits, a PLC procedure stops the pumps whenever the stack pressure drops exceed a given maximum limit (0.5 bar).
d. To avoid any secondary reaction or gas formation during charging at high SOC (~90%), a Labview procedure opens the main contactor in the case any cell voltage exceeds a maximum limit (1.65 V).
e. To prevent the occurrence of negative cell voltages, a Labview procedure opens the main contactor if any cell becomes lower than a given minimum limit (0.1 V) which can occur during deep discharges.

10. Early experimental results

The main components of the IS-VRFB, including stack, tanks, piping, instrumentation, PMS and BMS hardware with basic control functions, were installed in early 2017. After installation, the system underwent a long period of commissioning, in which many control, acquisition, processing and managing functions where developed and implemented and a number of ancillary devices where installed to provide noise suppression, reliable data acquisition and processing and safe control and operation. For the sake of example, special shielded inverter cables have been installed and placed inside copper pipes to limit the radiated and conducted electromagnetic noise which can affect the measurement chains. After several months of test operations, the system underwent extraordinary maintenance, the stack was opened and the internal state of each cell was carefully examined, to check their state of health. No siginficative

alteration was observed. In the same period the high current passive load was installed and tested. At present, the IS-VRFB has undergone about two months of experimental activities at high performance, during which the plant was tested in depth, the sensor system was completed, and more control and processing LabView procedures were implemented.

A LabView algorithm for computing the solution SOC from the open circuit voltage provided by the OCV cell was implemented. It is based on the Nernst equation expressed in terms of the SOC *s*:

$$E(s) = E^{0\,\prime} + \frac{2RT}{F} \ln \frac{s}{1-s} \tag{6}$$

where $E^{0\prime}$=1.37 V is the cell potential in standard condition at SOC=50%, i.e. corrected to account for the Donnan potential. Polarization curves were acquired at different SOCs and at a flow rate of 29.5 L min^{-1} (i.e. 1.23 mL min^{-1} per square centimeter of electrode active area), both in charge and discharge. Polarization and power curves both in charge and discharge at SOC 10%, 50%, and 90% are shown in Figure 7. During the execution of these experiments the solution temperature always remained between 20 °C and 28 °C.

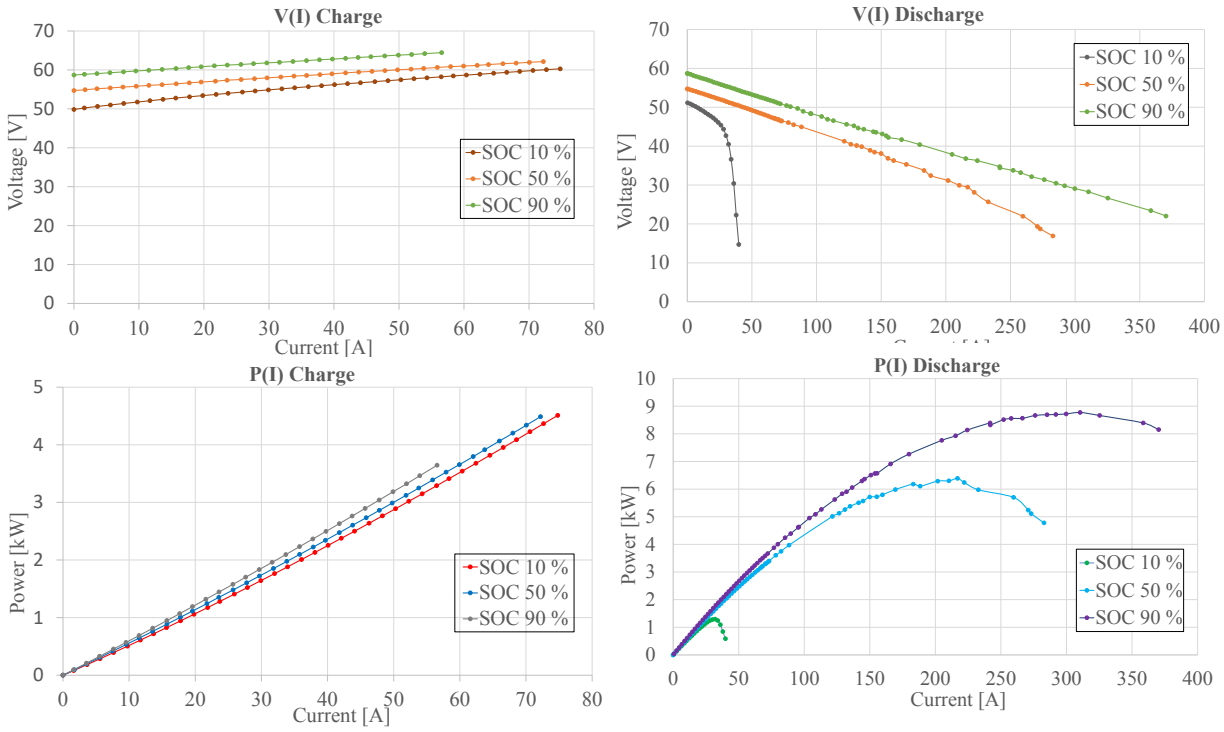

Figure 7. Stack polarization and power curves as a function of current at SOC 10%, 50%, 90% at flow rate of 29.5 L min^{-1} in charge (up to 75 A) and discharge (up to 75 A obtained with the controlled PMS and from 75 to 380 A obtained on the passive load).

Each data point was obtained by averaging some tens of measurements sampled between 5 and 20 seconds after starting the current. The 5 s delay was intended to minimize the effect of the initial overcurrents appearing at current startup before solution gradients stabilize inside the electrodes, whereas the total duration of 25 s was intended to limit SOC variations during the tests. In the first seconds of the acquisition period instantaneous currents were obviously higher than the reported average values. In the curves of Figure 7, points up to 75 A were obtained with the bidirectional PMS in both charge and discharge mode. Since 75 A is the rated current of the PMS both in charge and discharge, in order to extend experiments to higher discharge currents, a passive load consisting of variable resistors rated at 400 A was installed. The points between 75 A and 400 A in discharge operation of Figure 7 were obtained in this condition. They show that the maximum output power in discharge reached 8.9 kW, namely a pretty higher value that the design rate power of 4 kW. The weight of the stack filled with solutions is 115 kg so that the stack specific power density is 77 kW kg^{-1}.

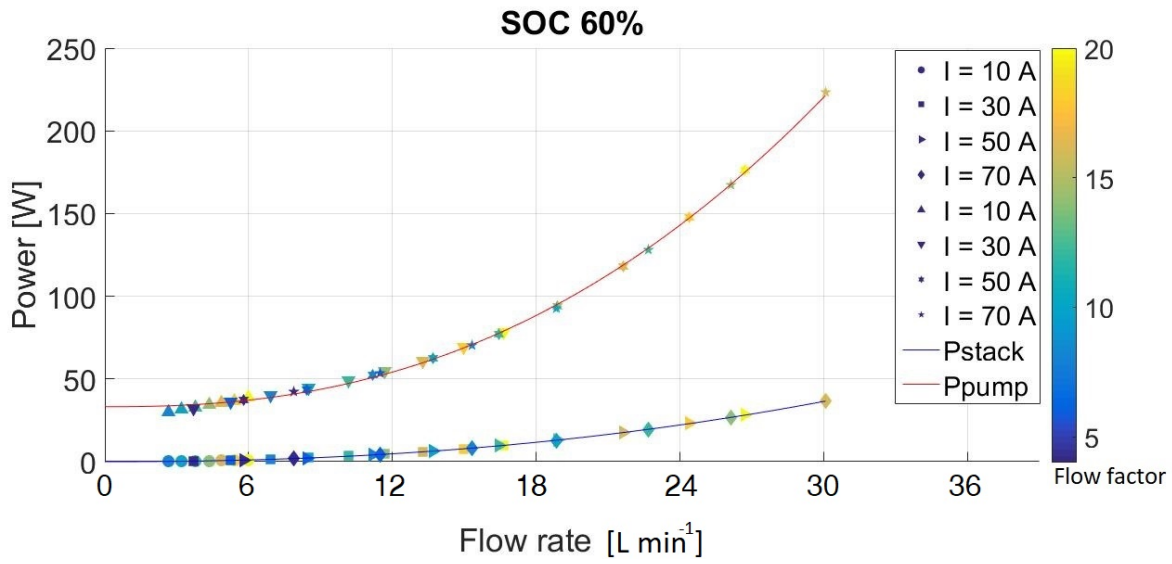

Figure 8. Hydraulic power losses Pstack and pumping power Ppump as function of the flow rate required at different current levels

Figure 7 also shows that at high SOC the polarization curves remain linear and the average cell voltage are above 0.5 V at 380 A, namely at 635 mA cm^{-2} while releasing a power of 8 kW. Also these values indicated a pretty good performance, considering that it was obtained in a 40-cell stack with active cross sectional areas as large as 600 cm^2. A next upgrade of the passive load will allow exploring the stack behavior at currents higher than 400 A, in order to approach the limiting current at which cell voltages vanish.

Early RTEs were also measured. In this case the tests were performed at constant current and constant flow factor $\alpha = 8$, charging and discharging the solutions between SOC 10% and 90%. The efficiency depends on the pumping power needed to compensate the hydraulic losses in the stack and piping which was measured with the power analyzer. Figure 8 shows how the hydraulic power losses in the stack P_{stack} and pumping power P_{pump} vary with the flow rate required at different current levels. The related pumping energy on the complete cycle has been taken into account in computing the RTE according to (4). The charge pumping energy $W_{pc} = 727$ Wh and discharge pumping energy $W_{pd} = 477$ Wh accounted for 3.5–4% of the respective energy flows W_c and W_d during a cycle at 30 A. In the case of a cycle at 70 A these figures reduced to 2.5–2.9%. The RTE resulted in 71% at 30 A and 62.5% at 70 A. It must be noted that flowmeters,

pressure gauge ports, valves, and piping geometry were responsible for localized losses which were evaluated to affect the RTE by about 2% and would be absent in a compact commercial design. In fact, for the sake of comparison, well-designed systems present minimized pumping power losses typically of 2–4% [48]. Accordingly, a RTE increase of 2% is at hand in a commercial design based on the same technology as IS-VRFB. Moreover, during early tests, the solution flow rates were not optimized at the electrical and chemical operating condition.

11. Conclusions

The IS-VRFB experiment has been recently completed and put into operation. In early tests a peak power close to 9 kW has been achieved, to be compared with the design value of 4 kW. The maximum tested current was 400 A corresponding to a current density of 665 mA cm^{-2} with a residual stack voltage of 18.5 V and output power of 7.4 kW. This performance is still below the stack limiting current, where stack voltage and power vanish. These early polarization and power data, together with preliminary RTE measurements in excess of 70%, prove a quite good design of the IS-VRFB cell and stack architecture, despite being provided with relatively thick carbon felt electrodes. Better performance is expected after the improvement of the hydraulic circuit and its control procedure and the upgrade of the electrical power circuitry. The experimental campaigns have just been started. However, these results demonstrate that the high current density so far reported only in small single-cell experiments can be transferred to larger industrial scale devices allowing for a notable reduction in system size and costs. Next programs include the execution of titration tests to accurately calibrate the $E(SOC)$ curve of (6) as well as the operation of the multichannel EIS to investigate the performance discrepancy among cells, as well as their aging effects. This information can address implementation of solution remixing on a programmed basis. A docking station for a short stack of smaller cells will allow to test new configuration of materials and flow designs and to compare them with the present stack.

12. Aknowledgement

This work was funded by the University of Padova under the strategic project MAESTRA 2011 “From Materials for Membrane-Electrode Assemblies to Electric Energy Conversion and Storage Device” (cod. STPD11XNRY 002) and the Project 2016 of the Interdepartmental Centre Giorgio Levi Cases for Energy Economics and Technology (GUAR_RICERCALASCITOLEVI17_02).

References

[1] M. Liserre, T. Sauter, J. Y. Hung, «Future energy systems: Integrating renewable energy sources into the smart power grid through industrial electronics,» *IEEE Ind. Electron. Mag.,* vol. 4, n. 1, pp. 18-37, March 2010.

[2] E. J. Coster, J. Myrzik, B. Kruimer, W. Kling, «Integration Issues of Distributed Generation in Distribution Grids,» *Proc. IEEE,* vol. 99, n. 1, pp. 28-39, Jan. 2011.

[3] T. Ackermann, G. Andersson, L. Söder, «Distribuited generation a definition,» *Electr. Pow. Syst. Res. ,* vol. 57, n. 3, pp. 195-204, Apr. 2001.

[4] T. Vu, K. Turitsyn, «Roboust transient stability assesment of renewable power grids,» *IEEE Int. Conf. Suistainable Energy Technologies (ICSET),* pp. 7-12, Jan 2016.

[5] M. Beaudin, H. Zareipour, A. Schellenberglabe, W. Rosehart, «Energy storage for mitigating the variability of renewable electricity sources: An updated review,» *Energy Sust. Dev.,* vol. 14, n. 4, pp. 302-314, Dec 2010.

[6] A. Evans, V. Strezov, T. Evans, «Assesment of utility energy storage options for increased renewable energy penetration,» *Renew. Sustain. Energy Rev.,* vol. 16, n. 6, pp. 4141-4147, Aug.2012.

[7] H. Chen, T. N. Cong, W. Yang, C. Tan, Y. Li, Y. Ding, «Progress in electrical energy

storage system: A critical review,» *Progr. Nat. Sci.,* vol. 19, n. 3, pp. 291-312, March 2009.

[8] N. Günter, A. Marinopoulos, «Energy storage for grid services and applications: Classification, market review, metrics, and methodology for evaluation of deployment cases,» *J. Energy Storage,* vol. 8, pp. 226-234, Nov. 2016.

[9] J. Cho, A. N. Kleit, «Energy storage systems in energy and ancillary markets: A blackwards induction approach,» *Appl. Energ. ,* vol. 147, pp. 176-183, June 2015.

[10] L. Müller, L. Viernstein, C. Truong, A. Eiting, H. Hesse, R. Witzmann, A. Jossen, «Evaluation of grid-level adaptability for stationary battery energy storage system applications in Europe,» *J. Energy Storage,* vol. 9, pp. 1-11, Feb. 2017.

[11] R. Hollinger, L. Diazgranados, F. Braam, T. Erge, G. Bopp, B. Engel, «Distributed solar battery systems providing primary control reserve,» *IET Renew. Power Gen.,* vol. 10, n. 1, pp. 63-70, Jan. 2016.

[12] F. Galiana, F. Bouffard, J. Arroyo, J. Restrepo, «Scheduling and Pricing of Coupled Energy and Primary, Secondary, and Tertiary Reserves,» *Proc. IEEE,* vol. 93, n. 11, pp. 1970-1983, Nov. 2005.

[13] W. Pickard, A. Q. Shen, N. J. Hansing, «Parking the power: Strategies and physical limitations for bulk energy storage in supply–demand matching on a grid whose input power is provided by intermittent sources,» *Renew. Sust. Energ. Rev.,* vol. 13, pp. 1934-1945, Oct. 2009.

[14] B. Dunn, H. Kamath, J. Tarascon, «Electrical Energy Storage for the Grid: A Battery of Choices,» *Science,* vol. 334, n. 6058, pp. 928-935, Nov. 2011.

[15] J. Kondoh, I. Ishii, H. Yamaguchi, A. Murata, K. Otani, K. Sakuta, N. Higuchi, S. Sekine, M. Kamimoto, «Electrical energy storage systems for energy networks,» *Energ. Convers.*

Manage., vol. 41, n. 17, pp. 1863-1874, 2000.

[16] P. Alotto, M. Guarnieri, F. Moro, «Redox Flow Batteries for the storage of renewable energy: a review,» *Renew. Sust. Energ. Rev.,* vol. 29, pp. 325-335, Jan 2014.

[17] B. Roberts, C. Sandberg, «The Role of Energy Storage in Development of Smart Grids,» *Proc. IEEE,* vol. 99, n. 6, pp. 1139-1144, June 2011.

[18] B. R. Chalamala, T. Soundappan, G. R. Fisher, M. Anstey, V. V. Viswanathan, M. L. Perry, «Redox Flow Batteries: An Engineering Perspective,» *Proc. IEEE ,* vol. 102, n. 6, pp. 976-999, 2014.

[19] J. Noack, N. Roznyatovskaya, T. Herr, P. Fischer, «The Chemistry of Redox-Flow Batteries,» *Angew. Chem. Int. Ed.,* vol. 54, p. 9776 –9809, 2015.

[20] I. Staffell, M. Rustomji, «Maximising the value of electricity storage,» *J. Energy Storage,* vol. 8, pp. 212-225, Nov. 2016.

[21] Z. G. Yang, «It's Big and Long-Lived, and It Won't Catch Fire: The Vanadium Redox-Flow Battery,» *IEEE Spectrum, Available at: https://spectrum.ieee.org/green-tech/fuel-cells/its-big-and-longlived-and-it-wont-catch-fire-the-vanadium-redoxflow-battery,* 26-Oct-2017.

[22] G. Spagnuolo, G. Petrone, P. Mattavelli, M. Guarnieri, «Vanadium Redox Flow Batteries: Potentials and Challenges of an Emerging Storage Technology,» *IEEE Ind. Electron. Mag.,* vol. 10, n. 4, pp. 20-31, 2016.

[23] L. H. Thaller, «Electrically rechargeable redox flow cells,» *NASA TM X-71540, Lewis Research Centre,* pp. 1-5, 1974.

[24] A. Pelligri, P. M. Spaziante, «in GB Patent 2030349 (1978), to Oronzio de Nori Impianti Elettrochimici S.p.A.».

[25] B. Sun, M. Skyllas-Kazacos, «A Study of the V(II)/V(III) Redox Couple for Redox Cell Application,» *J. Power Sources,* vol. 15, pp. 179-190, 1985.

[26] B. Sun, M. Rychik, M. Skyllas-Kazacos, «Investigation of the V(V)/V(IV) System for Use in the Positive Half-Cell of a Redox Battery,» *J. Power Sources,* vol. 16, pp. 85-95, 1985.

[27] L. Li, S. Kim, W. Wang, M. Vijayakumar, Z. Nie, B. Chen et al., «A stable vanadium redox-flow battery with high energy density for large-scale energy storage,» *Adv. En. Materials,* vol. 1, pp. 394-400, 2011.

[28] C. Choi, S. Kim, R. Kim, Y. Choi, S. Kim, H.-y. Jung, J. H. Yang, H.-T. Kim, «A review of vanadium electrolytes for vanadium redox flow batteries,» *Renew. Sust. Energ. Rev.,* vol. 69, n. 1, pp. 263-274, 1 2017.

[29] M. Skyllas-Kazacos, L. Cao, M. Kazacos, N. Kausar, A. Mousa, «Vanadium Electrolyte Studies for the Vanadium Redox Battery—A Review,» *ChemSusChem Reviews,* vol. 9, n. 1, p. 1521–1543, 1 2016.

[30] L. Li, S. Kim, W. Wang, M. Vijayakumar, Z. Nie, B. Chen, J. Zhang, G. Xia, J. Hu, G. Graff, J. Liu, Z. Yang, «A stable vanadium redox-flow battery with high energy density for large-scale energy storage,» *Adv. En. Materials,* vol. 1, n. 3, pp. 394-400, 1 2011.

[31] W. Wang, Q. Luo, B. Li, X. Wei, L. Li, Z. Yang, «Recent progress in redox flow battery research and development,» *Adv. Funct. Materials,* vol. 23, n. 8, pp. 970-986, 1 2013.

[32] R. A. Elgammala, Z. Tanga, C.-N. Sunb, J. Lawtona, T. A. Zawodzinski Jr., «Species Uptake and Mass Transport in Membranes for Vanadium Redox Flow Batteries,» *Electrochimica Acta,* vol. 234, pp. 1-11, 2017.

[33] X. Zhou, T. Zhao, L. An, Y. Zeng, X. Zhu, «Performance of a vanadium redox flow battery

with a VANADion membrane,» *Appl. Energ.,* vol. 180, pp. 353-359, 2016.

[34] Y. Lei, B. Zhang, Z. Zhang, B. Bai, T. Zhao, «An improved model of ion selective adsorption in membranes and its application in vanadium redox flow batteries,» *Appl. Energ.,* vol. 215, pp. 591-601, 2018.

[35] X.L. Zhou, T.S. Zhao, L. An, Y.K. Zeng, L. Wei, «Modeling of ion transport through a porous separator in vanadium redox flow batteries,» *Journal of Power Sources,* vol. 327, pp. 67-76, 2016.

[36] A. M. Pezeshki, R. L. Sacci, F. M. Delnick, D. S. Aaron, M. M. Mench, «Elucidating effec of cell architecture, electrode material, and solution composition on overpotentials in redo flow batteries,» *Electrochimica Acta ,* vol. 229, p. 261–270, March 2017.

[37] Q. Wang, Z. Qu, Z. Jiang, W. Yang, «Experimental study on the performanceof a vanadium redox flow battery with non-uniformly compressed carbon felt electrode,» *Appl. Energ.,* vol. 213, pp. 293-305, 2018.

[38] O. Di Blasi, N. Briguglio, C. Busacca, M. Ferraro, V. Antonucci, A. Di Blasi, «Electrochemical investigation of thermically treated graphene oxides as alectrode materials for vanadium redox flow battery,» *Appl. Energ.,* vol. 147, pp. 74 - 81, 2015.

[39] S. Abbas, H. Lee, J. Hwang, A. Mehmood, H.-J. Shin, S. Mehboob, J.-Y. Lee, H. Y. Ha, «A novel approach for forming carbon nanorods on the surface of carbon felt electrode by catalytic etching for high-performance vanadium redox flow battery,» *Carbon,* vol. 128, pp. 31-37, 2018.

[40] X.L. Zhou, T.S. Zhao, Y.K. Zeng, L. An, L. Wei,, «A highly permeable and enhanced surface area carbon-cloth electrode for vanadium redox flow batteries,» *Journal of Power Sources,* vol. 329, pp. 247-254, 2016.

[41] Q. Xu, T. Zhao, C. Zhang, «Performance of a vanadium redox flow battery with and withoutflow fields,» *Electrochimica Acta,* vol. 142, pp. 61-67, 2014.

[42] M. Messaggi, P. Canzi, R. Mereu, A. Baricci, F. Inzoli, A. Casalegno, M. Zago, «Analysis of flow field design on vanadium redox flow battery performance: Development of 3D computational fluid dynamic model and experimental validation,» *Appl. Energ.,* vol. 228, pp. 1057-1070, 2018.

[43] Q. Xu, T. Zhao, P. Leung, «Numerical investigations of flow field designs for vanadium redox flow batteries,» *Appl. Energ.,* vol. 105, pp. 47-56, 2013.

[44] D.S. Aaron, Q. Liu, Z. Tang, G.M. Grim, A.B. Papandrew, A. Turhan, T.A. Zawodzinski, M.M. Mench, «Dramatic performance gains in vanadium redox flow batteries through modified cell architecture,» *J. Power Sources,* vol. 206, pp. 450-453, 2012.

[45] D.-J. Park, K.-S. Jeon, C.-H. Ryu, G.-J. Hwang, «Performance of the all-vanadium redox flow battery stack,» *Journal of Industrial and Engineering Chemistry,* vol. 45, pp. 387-390, 2017.

[46] T. Shigematsu, «Redox flow battery for energy storage,» *SEI Tech. Rev.,* n. 73, pp. 4-13, 2011.

[47] M. Schreiber, M. Harrer , A. Whiteheadb, H. Bucsicha, M. Dragschitz, E. Seifert, P. Tymc, «Practical and commercial issues in the design and manufacture of vanadium flow batteries,» *J. Power Sources,* vol. 206, pp. 483-489, 2012.

[48] L. Arenas, C. Ponce de Leon, F. Walsh, «Engineering aspects of the design, construction and performance of modular redox flow batteries for energy storage,» *Journal of Energy Storage,* vol. 11, pp. 119-153, 2017.

[49] «Fraunhofer Institute of Chemical Technology ICT, "Redox Flow Battery,",» *available https://www.ict.fraunhofer.de/en/comp/ae/rfb.html,* retrieved on 20/03/2018.

[50] J. Noack, C. Cremers, D. Bayer, J. Tübke, K. Pinkwart, «Development and characterization of a 280 cm2 vanadium/oxygen fuel cell,» Journal of Power Source, vol. 253, pp. 397-403, 2014.

[51] Dong-Jun Park, Kwang-Sun Jeon, Cheol-Hwi Ryu, Gab-Jin Hwang, «Performance of the all-vanadium redox flow battery stack,» *Journal of Industrial and Engineering Chemistry,* vol. 45, p. 387–390, 2017.

[52] S. Kim, E. Thomsen, E. Xia, N. J. J. Bao, K. Recknagle, W. Wang, V. Viswanathan et al., «1kW/1kWh advanced vanadium redox flow battery utilizing mixed acid electrolytes,» *J. Power Sources,* pp. 300-309, 2013.

[53] F. Moro, A. Trovò, S. Bortolin, D. Del Col, M. Guarnieri, «An alternative low-loss stack topology for vanadium redox flow battery: Comparative assessment,» *J. Power Sources,* vol. 340, pp. 229-241, 2017.

[54] R. M. Darling, M. L. Perry, «The Influence of Electrode and Channel Configurations on Flow Battery Performance,» *Journal of The Electrochemical Sociecty,* vol. 161, p. 9, 2014.

[55] D. Maggiolo, F. Zanini, F. Picano, A. Trovò, S. Carmignato, M. Guarnieri, «Particle based method and X-ray computed tomography for pore-scale flow characterization in VRFB electrodes,» *Energy Storage Materials,* vol. 16, n. 1, pp. 91-96, 1 2019.

[56] C. Chang, H. Chou, N. Hsu, Y. Chen, «Development of integrally molded bipolar plates for All-Vanadium Redox Flow Batteries,» *Energies,* vol. 9, n. 5, pp. 1-10, 2016.

[57] N. Soohyun, L. Dongyoung, C. Ilbeom, L. Dai Gil, «Smart cure cycle for reducing the

thermal residual stress of a co-cured E-glass/carbon/epoxy composite structure for a vanadium redox flow battery,» *Composite Structures,* vol. 120, pp. 107-116, February 2015.

[58] H. Nakaishi, T. Kanno, S. Ogino, T. Ito, T. Shigematsu, N. Tokuda, «Cell frame for redox-flow cell and redox-flow cell». US Patent 20040202915, 2004.

[59] H. Nakaishi, T. Kanno, S. Ogino, T. Ito, T. Shigematsu, N. Tokuda, «Cell frame for redox flow battery, and redox flow battery». US Patent 20080081247, 2008.

[60] H. Nakahata, N. Ayai, T. Shibata, «Development of Smart Grid Demonstration Systems,» *SEI TECHNICAL REVIEW,* vol. 76, p. 8–13, 2013.

[61] X. Ma, H. Zhang, C. Sun, Y. Zou, T. Zhang, «An optimal strategy of electrolyte flow rate for vanadium redox flow battery,» *J. Power Sources,* vol. 203, pp. 153-158, 2012.

[62] B. Xiong, J. Zhao, K. J. Tseng, M. Skyllas-Kazacos, T. M. Lim, Y. Zhang, «Thermal hydraulic behaviour and efficiency analysis of an all-vanadium redox flow battery,» *J. Power Sources,* vol. 242, pp. 314-324, 2013.